Seismicity Detection in Skopje Region Using Tomographic Methods and 3-D Modelling

Cvetan Sinadinovski[1], Lazo Pekevski[2], Dragana Cernih[3], Katerina Drogreska[4], and Jasmina Najdovska[5]

1. Corresponding Author. Director, Global SeismiCS, Canberra ACT, Australia. Email: cvetansin@hotmail.com

2. frm Associate Professor, Seismological Observatory, PMF, University "Ss. Cyril and Methodius" (UKIM), Skopje, Macedonia. lazopekevski@yahoo.com

3. Seismological Observatory, PMF, University "Ss. Cyril and Methodius" (UKIM), Skopje, Macedonia. dcernih@gmail.com

4. Seismological Observatory, PMF, University "Ss. Cyril and Methodius" (UKIM), Skopje, Macedonia. katerinadrogreska@yahoo.com

5. Seismological Observatory, PMF, University "Ss. Cyril and Methodius" (UKIM), Skopje, Macedonia. najdovskaj@yahoo.com

Abstract

A novel geotomography technique was applied at the epicentral area around capitol of Macedonia - Skopje, using selected earthquakes that occurred over a period of 57 years and were recorded on temporary and permanent seismograph stations. This study tested a tomography suite for the first time in investigation of the crustal shape and structures in a complex tectonic environment. Special datasets were designed for that purpose, covering two periods: 1964-1967 and 2016-2020.

In the initial phase, the analysis shows the potential of the geotomography application in revealing detailed velocity perturbation in the lithosphere. Then, the events are relocated in the 3-D models and new cross-sections of the crust produced by a simultaneous approach. The images help in constraining the velocity vs depth relationship and thus can contribute towards redefinition of the earthquake zones. The results are discussed in terms of the general seismic regime and the temporal and spatial changes.

Better understanding of the seismicity and tectonics processes in the Skopje region will also lead to an overall improvement of the earthquake hazard assessment at local and national level, as well as further integration in research programs with other geophysical methods.

Keywords: earthquakes, velocity modelling, inversion, seismic tomography

1 INTRODUCTION

A series of tests with a novel geotomographic software were performed to investigate the seismotectonic features and crustal structure in an active tectonic region - the Skopje epicentral area in Macedonia. The 3-D models and the cross-sections of the crust produced by this methodology showed the potential of the geotomography application in revealing velocity perturbation in the lithosphere (Sinadinovski *et al.,* 2020). These new images will constrain the velocity versus depth relationship and contribute towards better relocation of earthquakes, which will lead to an improvement of the earthquake hazard assessment programs (for instance UNDP/UNESCO).

Two recently compiled datasets of local earthquakes which occurred in the periods 1964-1967 and 2016-2020, recorded on seismic stations in the wider region around Skopje, were used as input into the tomography program. The seismologists at the Skopje Seismological Observatory selected the events based on the quality of the arrivals read from the seismograms. Out of many recordings, after careful inspection, some 40 earthquakes from the 1960's period and 100 earthquakes from the 2010's period were chosen for the tomography experiment.

In our method, we first inverted the travel-times from all the source-receiver combinations to calculate the propagation times of seismic rays and compared the arrival times with the theoretical forward modelling. Then the difference between the theoretical calculations and the observed times was minimised and at the end, we performed separate tests with various 3-D velocity models in order to monitor their effect on the location accuracies.

With the new tomography suite, we can display a variety of images. These include: the velocity or slowness perturbations in respect to a reference velocity model, horizontal or vertical slices through the volume, seismic ray density through the grid mesh and refinement of discretization among others.

2 METHODOLOGY

In seismic tomography, the time of the seismic waves travelling between the focus of the earthquake and the station is measured and used in an inversion process, referred to as "travel-time inversion". The surveyed volume, the cuboid, is discretised into cells of a certain grid size on the surface and depth ranges in chosen intervals. Within the cuboid, for each source-receiver i.e. earthquake-station combination, the travel-time is calculated based on the initial velocity model. Then the calculated arrivals are compared with the observed arrivals on the seismograms, commonly for the P and S-phases (for example, Kennett and Abdullah, 2011).

The tomographic inversion is performed using irregular grid parametrization; tetrahedron cell discretization (Fig. 1a) of complex geological models is especially useful in situations of rough topography and high-contrast anomalies. Tetrahedron ribs are utilized for ray tracing that are finer at shallow depths and coarser at greater depth (Fig. 1b). Source and receiver locations are embedded into the ribs to enable ray tracing between each source and receiver pair. Our approach allows fast iterations for geometry with narrow offset (local earthquakes) as well as inclusion of the more distant earthquakes in reduced computation time (Sinadinovski *et al.,* 2019a).

Furthermore, the search for finding the nearest neighbours of a specific number of points is used to optimize the algorithm during searching for the fastest path that fulfills the Fermat principle. Therefore, forward models are more realistic and the resulting images of the sub-structures can indicate variations in the velocity with a higher degree of resolution.

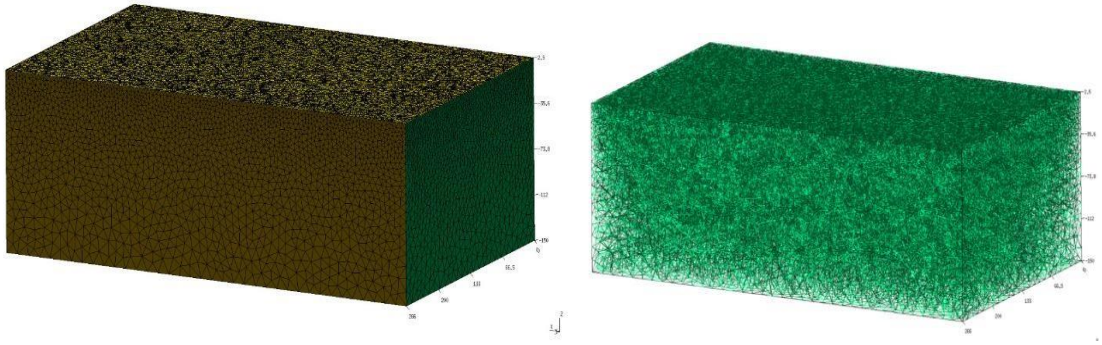

a) b)

Figure 1 Schematic representation of a) grid parametrization and b) tetrahedron ribs used for ray tracing. (Model size is relative and numbers can be scaled up or down).

The tomography calculations are stored as a matrix of velocity values and slowness perturbations in respect to the initial model. The images can be graphically shown at various slices through the cuboid, typically horizontally (depth) and vertically (longitude and latitude). The novelty of our approach over the previous tools is its ability to be applied simultaneously in forward modelling and inversion, thus allowing the user to monitor in 3-D space the effects of the re-location of seismic events by the model composition.

The inverse problem of earthquake relocation can be described using relationship of data $\boldsymbol{d}$ and model parameter $\boldsymbol{m}$:

$$\boldsymbol{d} = \boldsymbol{g}(\boldsymbol{m}) \qquad \text{(Eq. 1)}$$

where $\boldsymbol{d}$ matrix is travel time, $\boldsymbol{m}$ is the hypocenter location (x_0, y_0, z_0) and $\boldsymbol{g}$ is the velocity model. The calculated travel time $\boldsymbol{d}$ could be modified by adjusting the hypocenter location for given velocity models. The solution will converge as the travel time in the model ($\boldsymbol{d_m}$) comes close to the travel time of observation ($\boldsymbol{d_{obs}}$).

Since the inverse problem is a non-linear by nature, to reach convergence we adopted non-linear approximation of a Fast Marching Method – FMM, to predict the travel time in 3-D grid volume with inhomogeneous medium velocity (A. Abdullah's group, *personal communications, 2020*). The new hypocenter location is obtained by minimizing the objective function $S(\boldsymbol{m})$ defined by Eq.2:

$$S(\boldsymbol{m}) = (\boldsymbol{d}_{obs}^r - \boldsymbol{d}_m^r)^T(\boldsymbol{d}_{obs}^r - \boldsymbol{d}_m^r) \qquad \text{(Eq. 2)}$$

where $\boldsymbol{d}_{obs}^r$ is a vector $(N \times 1)$ matrix containing observed arrival times of N stations with the mean subtracted, and $\boldsymbol{d}_m^r$ is a same size vector matrix containing predicted travel times from FMM, also with the mean subtracted (Rawlinson, 2008). Thus, the result of Eq.2 matrix multiplication should be a single value of the scalar objective function for one grid point.

The reciprocity principle is used to build the travel time model ($\boldsymbol{d_m}$), where the station is considered a source and then predict the travel time for every grid point using FMM for given velocity models, in our case the output after the final inversion.

In resolving Eq.2, for every grid points we performed the multi-dimension matrix multiplication (vectorization) instead of looping. A 3-D medium matrix was considered with size ($I \times J \times K$) corresponding to (x, y, z) coordinates. Regarding the reciprocity principle, the travel time model was built for every station, for instance (M) the number of stations and a 4-D matrix ($I \times J \times K \times M$) was formed of the travel time model ($\boldsymbol{d_m}$). By taking the travel time observation ($\boldsymbol{d_{obs}}$) into account, the residual travel time of observed and model ($\boldsymbol{d_{obs}} - \boldsymbol{d_m}$) matrix is obtained with size ($I \times J \times K \times M$). Finally, by adapting Eq.2, we calculated the objective function $S(\boldsymbol{m})$ as a 4-D matrix multiplication resulting of 3-D matrices ($I \times J \times K$) of the objective functions.

In order to obtain more accuracy when the station coordinates fall between the grid points, we performed a 3-D interpolation of the FMM results to build the travel time model. First, we specified a voxel proportional to the grid spacing around the station location and then interpolated the travel times between its 8 points until the actual position of the station is covered.

The last step was to find the minimum value of the objective function. We assumed that the minimum value is located within the grid. Therefore, to have more accurate locations, we applied gradient descent and damping to minimize the misfit function for every voxel.

In tomography, there is always a trade-off between the grid size or refinement and the misfit function which depends on many input parameters during the iterations. *A priori* assumptions in geology can help in constraining the velocity model, so researchers need to find the best combination of parameters to suit the geological conditions.

3 SYNTHETIC TESTS

Earlier, we designed a few synthetic datasets to test the sensitivity of the input parameters and to fine-tune them in search of optimal results (Sinadinovski *et al.*, 2019a). One simple case of a discretized volume 2.5°x2.5° with five layers containing 11 events (red dots) recorded on 5 stations (green dots) is presented on Figure 2.

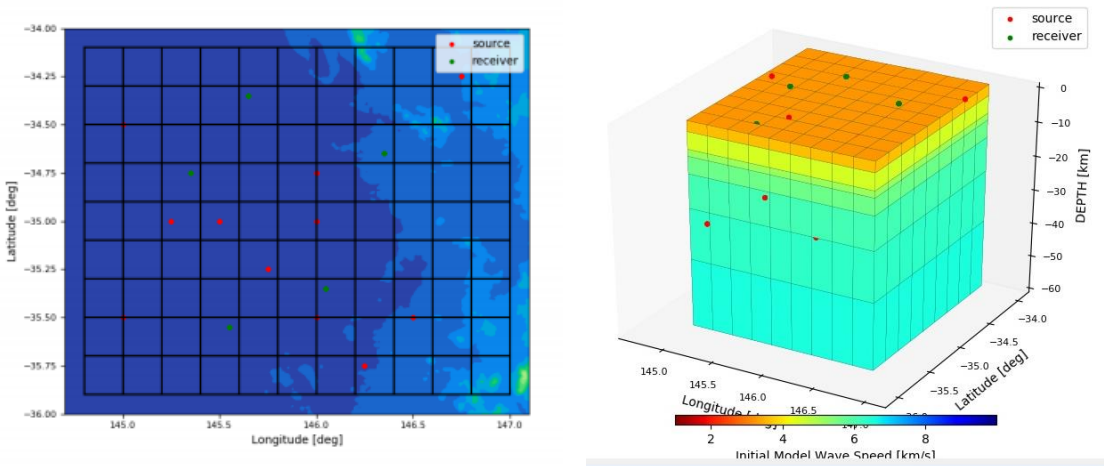

Figure 2 Synthetic model for testing the sample topography (left) and the 3-D V_p model (right).

The so-called checkerboard test was performed first, in which the cells of alternating high- and low-velocity values were placed in each layer. The recovered image for the rays from all the source-receiver pairs gave an indication of the ability of the program to detect velocity variations. A ray count was run automatically in parallel and the results were monitored for each stage of the calculation. Figure 3 displays the ray coverage and recovered checkerboard for one chosen cross-section in vertical direction.

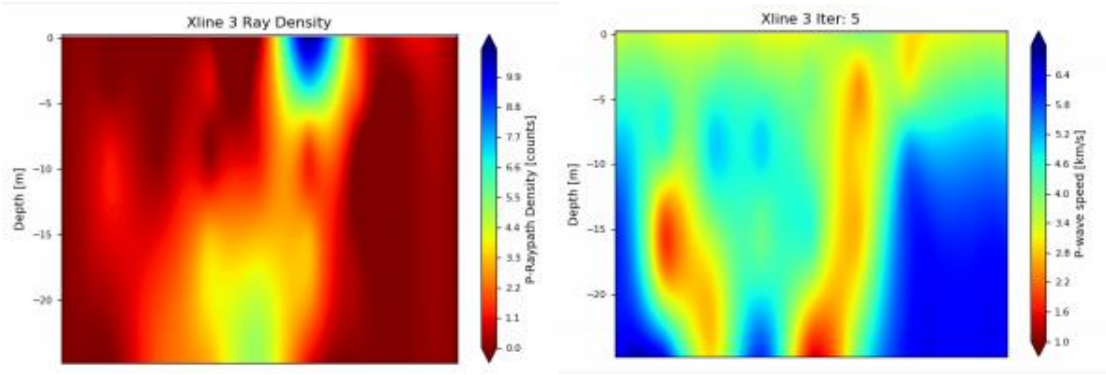

a) b)

Figure 3 Visualization of: a) the ray coverage and b) the recovered checkerboard image for one latitudinal slice through the synthetic model.

The P- and S-arrival data were created with forward modelling. An assumed random error of +/-0.1s was introduced to the calculated times, which is about the reading error of phases from seismograms. We did multiple runs with the tomography program to monitor the influence of the parametrization on the output images. Figure 4 shows the ray coverage and recovered field data image for a horizontal cross-section at a depth of 4km.

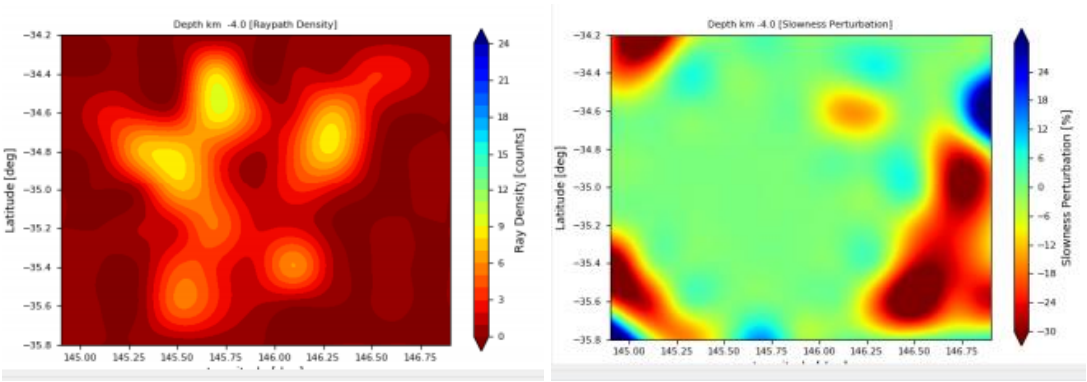

a) b)

Figure 4 Visualization of: a) the ray coverage and b) the recovered image with field data, for one horizontal slice through the synthetic model.

The results of the tomography inversion are reliable only in areas with good ray coverage. For example, in Fig. 4, just the part within the star-shaped area is sufficiently well covered by rays, outside the star ray paths are influenced by artefacts. Voxels which were not criss-crossed by rays were set to their initial values in the velocity model, because no extra information was available.

In general, the tomographic images are better resolved under the network of stations, while the uncertainty increases with the distance from the closest recording station. Also, a good azimuthal coverage is important, since the station configuration aligned at one side of the zone where events occur may cause spurious effects in calculation of their spatial location.

Attempts were made to test the relocation of events within the 3-D synthetic model with the procedure described in the earlier section 2. The grid size and the nodes refinement were varied from cases with large spacing down to just ±1km, though the smallest spacing consumed a large amount of computer CPU memory. The coordinates of the original events were compared with the relocated events and differences saved in the associated output directory. Figure 5 shows the distribution of the original (orange points) versus the relocated events (blue points).

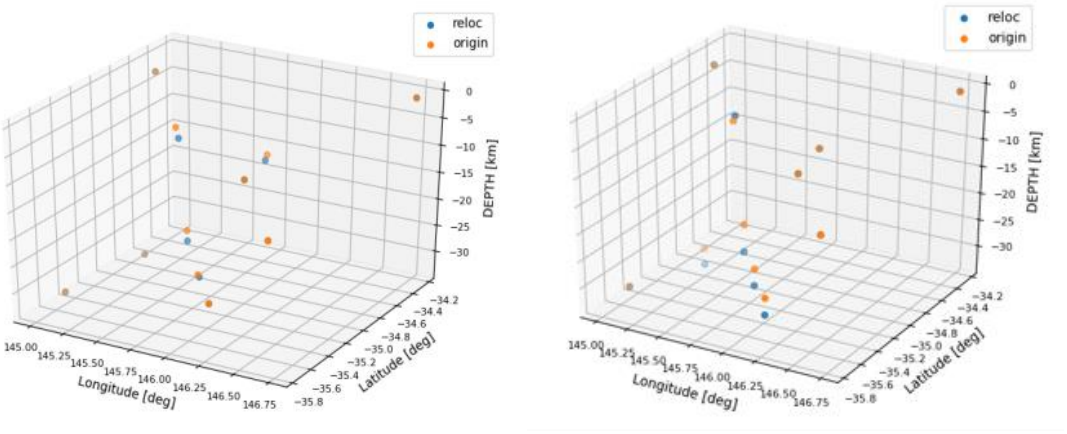

a) b)

Figure 5 Distribution of the original versus relocated events when: a) the maximum difference was limited to ±6km and b) the maximum difference was not limited.

The results of the relocation are strongly dependent on the 3-D velocity model, especially on its near surface layers. If the tomography model is too far from the initial model used to generate the arrival times, then the calculation of the objective function is stacked in the local minima and gives unrealistic solutions.

4 FIELD DATA TESTS FOR THE SKOPJE EPICENTRAL AREA

Two acquired data sets consisted of picked P- and S- arrivals from the seismograms collected from the seismic stations deployed in the Skopje epicentral area to record earthquakes in the periods of 1964-1967 and 2016-2020 (Table 1). For the tomography experiment, we selected around 40 local earthquakes from the older period and 100 earthquakes from the more recent period, which satisfied the criteria of having clear arrival times readings on the seismograms and their epicenters were in the radius of 35km from the city center. Some 100 P-arrival times and a corresponding number of S-arrival times were used in the tomographic analysis for the first period and around 300 P- and S- arrivals for the later period.

Table 1 Recording stations' coordinates (1964-1967 left and 2016-2020 right).

Stn Code	λ	φ	Elev. (km)		Stn Code	λ	φ	Elev. (km)
SKO	21.44	41.972	0.346		SKO	21.44	41.972	0.346
BRA	21.403	42.075	0.391		KOZJ	21.195	41.878	0.533
MYG	21.301	41.957	0.306		LIS	21.612	41.679	0.42
LIP	21.583	42.162	0.483		OTOV	21.753	41.779	0.265
KAY	21.702	41.896	0.248		BELI	21.274	41.683	0.523
					SVPE	21.26	41.922	0.449

The events that occurred in a cuboid of 21.1ºE to 21.75ºE and 41.6ºN and 42.2ºN and down to 60km deep were processed. The volume was discretised into a 5km x 5km grid cells in the surface area and depth ranges in the intervals from 5, 10, 15, 20, 30, 45 and 60km. To investigate the 3-D structure underneath the Skopje epicentral area, the initial velocity model (after Pekevski *et al.*, 2009) was utilised from the HypoInv program as shown in Table 2. Figure 6 shows the three-dimensional P-wave velocity model for the experiment. This set-up allowed to maximise the imaging of the top layers, evaluate the discontinuity depth and detect the patterns of seismicity.

Table 2 Velocity model used for locating earthquakes in the Skopje region.

Depth (km)	Vp (km/s)	Vs (km/s)
0-5	4.4	2.54
5-10	5.1	2.95
10-15	6.2	3.58
15-20	6.5	3.76
20-30	6.9	3.99
30-45	7.7	4.45
45-60	8.045	4.65

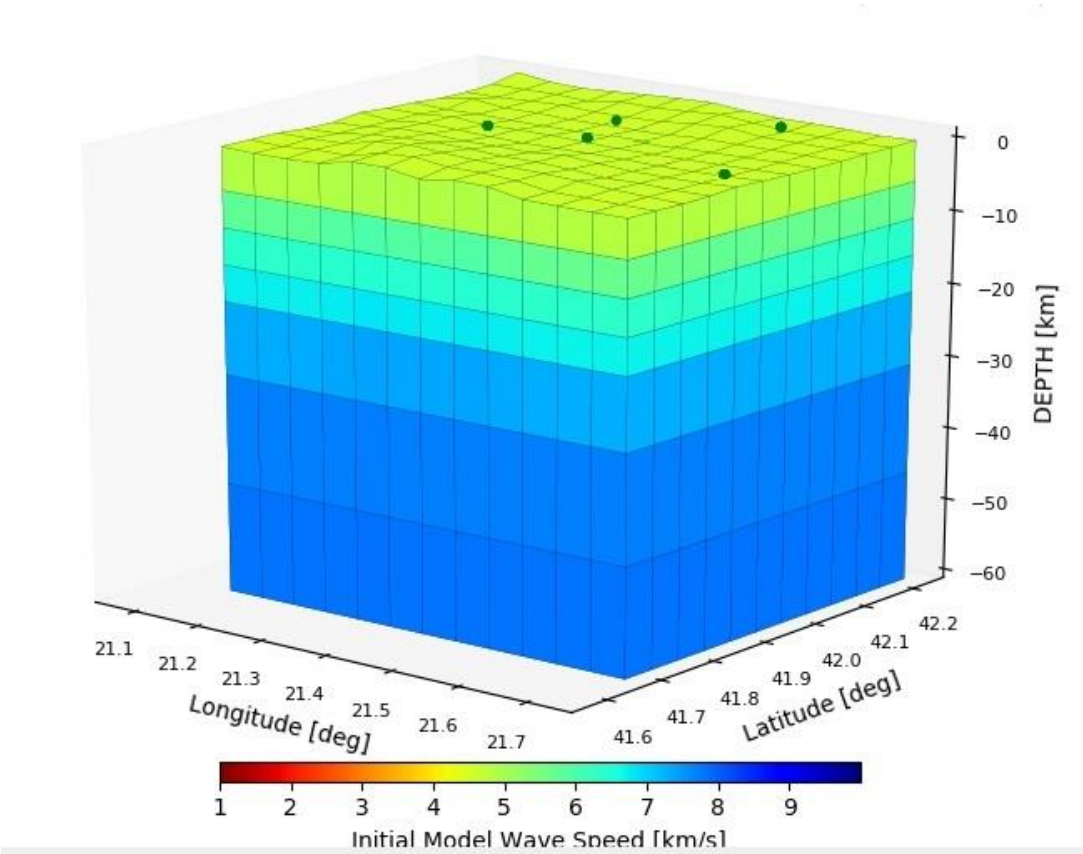

Figure 6 Layered velocity model V_p used for the Skopje region – the 3-D view (stations depicted as green dots).

Period 1964-1967

A network of temporary seismic stations was deployed specifically after the devastating Skopje 1963 earthquake, with aim to detect the aftershocks in its epicentral area, and was operational for about four years. We started our study by retrieving the archived data from the 1964-1967 period and selected the strongest detected events. They are shown on top of figure 7, while the schematic ray paths between the sources/hypocenters and the receivers/stations are displayed on the bottom.

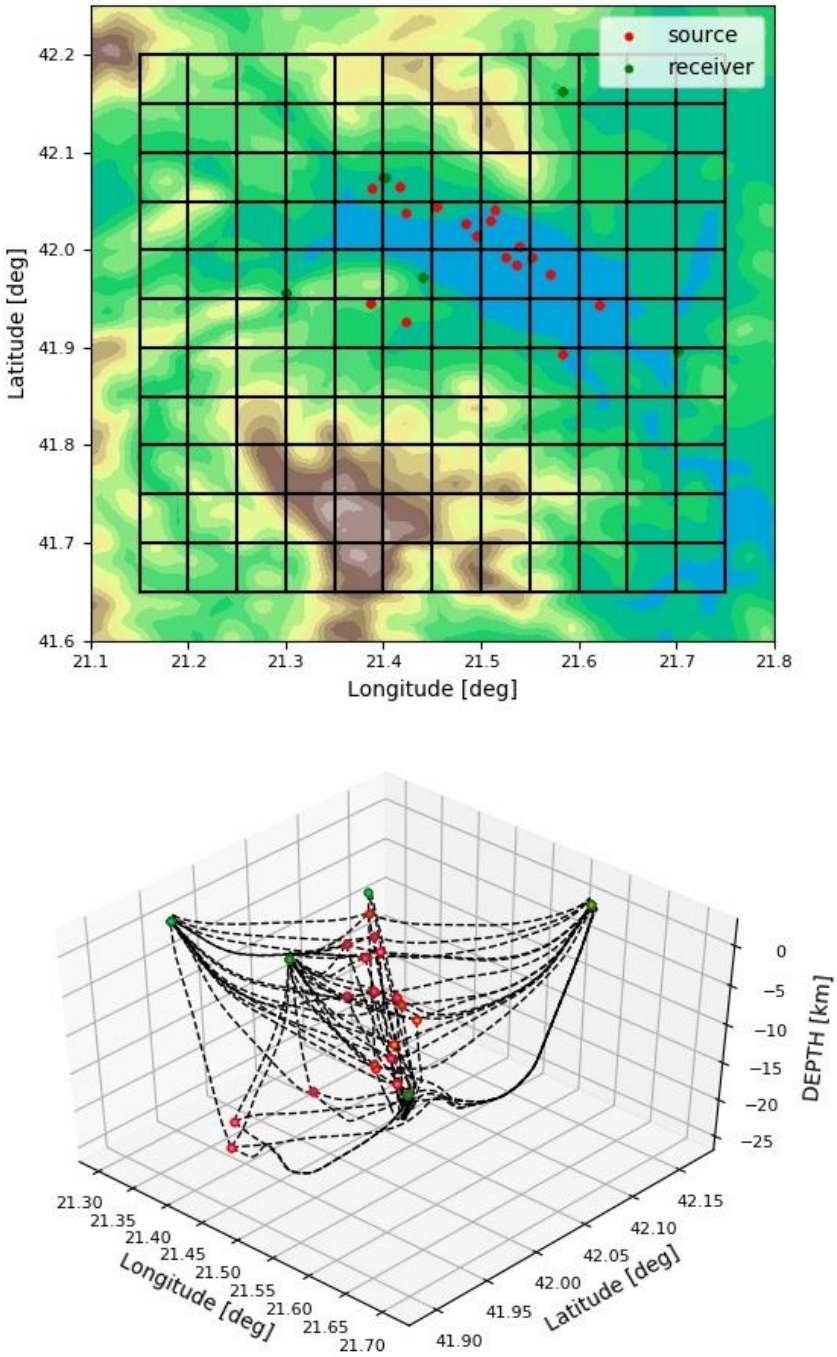

Figure 7 Seismicity of the Skopje region for the period 1964-1967: top – epicenters and stations superimposed on topography map; and bottom – ray paths between sources and receivers.

The results for each stage are done in windows with dynamic resizing, so the discretized volume, the events, the cross-sections and the rays can be displayed in a user-defined frame. The model misfit function was monitored for each inversion and for the data from the 1964-1967 period, it was usually found to converge steadily to a minimum after just a few iterations, when the tolerance level was set to half of the reading error.

The trials with the tomography package started with the checkerboard tests and the latitudinal and longitudinal slices through the initial velocity model. Out of many tests, we decided to display here the E-W and N-S slices that intersected closest to an approximate city center point (Figure 8).

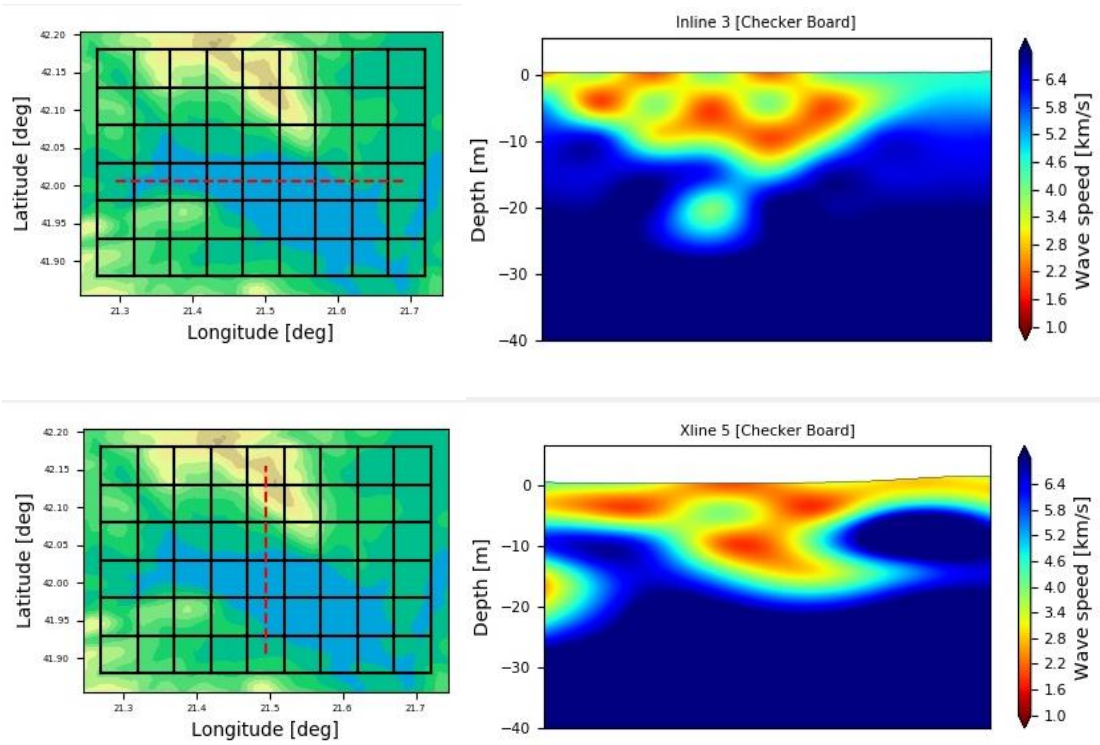

Figure 8 Recovered checkerboard images for the slices (dashed line on the left side) in respect to the initial velocity model; (Blue-fast, Red-Slow).

The most southerly slices in the cuboid had insufficient ray coverage to change the background velocity model. The images produced using the P- and S-arrivals look very similar, due to the fact that the number of readings used in the inversion was very close in both cases. The results from the second to the fifth slice of the cuboid can be viewed with higher confidence because they had relatively good angular coverage. As the deepest earthquake data used in the 1964-1967 period analysis was down to 25km, only the voxels in the top 30km part of the volume were covered by the rays. Thus, the deeper section may experience the artefacts of tomography. Voxels in the bottom layer which were not criss-crossed by rays were left unchanged to their initial values in the velocity model, because no extra information was available.

Then, we produced the tomography images with the field data for the selected longitudinal and latitudinal sections through the model. The same two E-W and N-S slices that intersected closest to the point 42°N and 21.5^{o}E were considered for comparison. Tomography slices can also be represented in other directions or as a relative slowness perturbation in terms of a percentage within the layers, as shown on Figure 9.

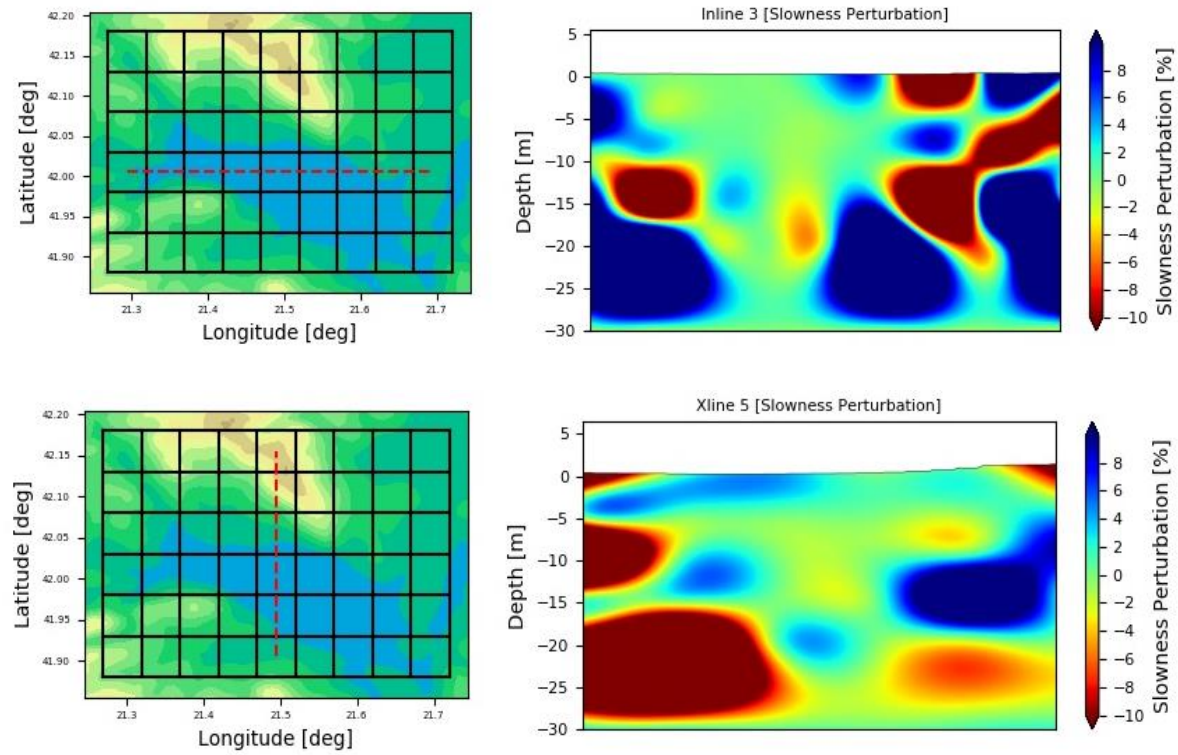

Figure 9 Slowness perturbation images of field data for the slices (dashed line on the left side) as percentage values from the initial velocity model; (Blue-High, Red-Low).

So far, with tomography we have used the data to image the volume in 3-D, detect layers in the crust and evaluate possible discontinuity. In the following step, the output velocity model from tomography was employed to relocate the seismic events. Multiple combinations of initial models and arrival times types were used in the relocation process. The first series of computer runs was completed using the extended 1-D models of Table 2 into layers of constant velocity. The second series of runs was done with a computer generated 3-D model consisting of interpolated velocity values from the initial model, used at the start of iterations. Both series were performed with the selected P- and S-arrival times. Sample distribution of the original versus relocated events for two search spacings and picking precision of $\pm$0.1s is presented on Fig. 10.

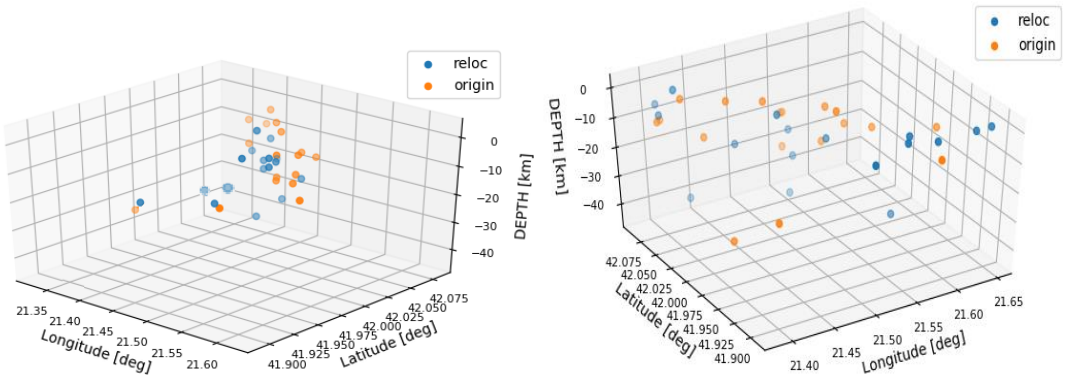

Figure 10 Distribution of the original (orange dots) versus relocated (blue dots) events for search spacing steps of 3km (left) and 1km (right) using the extended 1-D model with P-arrivals. (Mixed colour dots when original and relocated position coincided).

Preliminary observations from our tomography images and the event relocation indicated that the initial velocity in the third and fourth layer (10-20km) was higher by 5%, which caused a downwards trend of the relocated events underneath the Skopje Valley. That is in line with the previous remarks that the results are strongly influenced by the geology of the top layers. Consequently, such proxy 3-D model based on the extended 1-D model is more appropriate to be used locally in the smaller scale studies.

Period 2016-2020

After 2000, a network of digital seismic stations was installed to monitor the seismicity in the Skopje epicentral area. It has been operational for about fifteen years and is capable to detected both big and small events. The study continued by selecting the data from the 2016-2020 period, which included the strong Skopje earthquake magnitude M_L5.3 that occurred in September of 2016. The epicenters are shown on top of figure 11, while their schematic source-receiver ray paths are displayed below it.

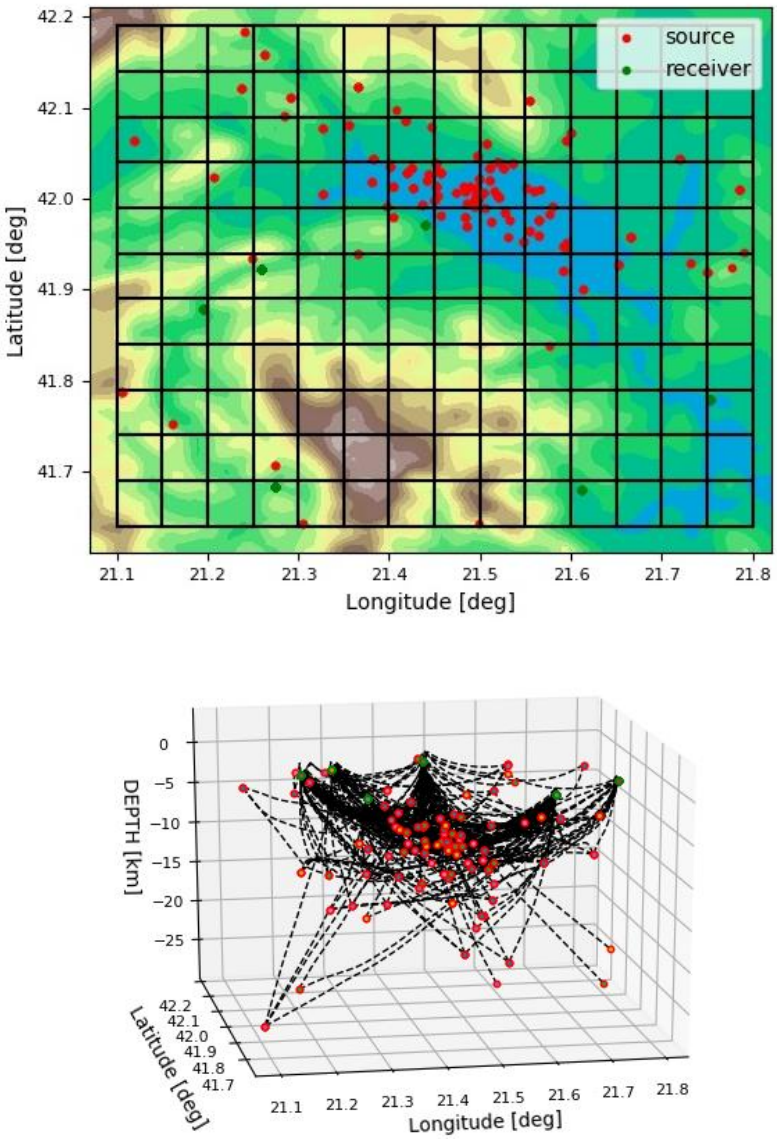

Figure 11 Seismicity of the Skopje region for the period 2016-2020: top – epicenters and stations superimposed on topography map; and bottom – source-receiver ray paths.

The model misfit function was monitored for each inversion and for the data from the 2016-2020 period, it was also found to converge steadily to a minimum after just a few iterations, when the tolerance level was set to half of the reading error (typical shape displayed on Figure 12).

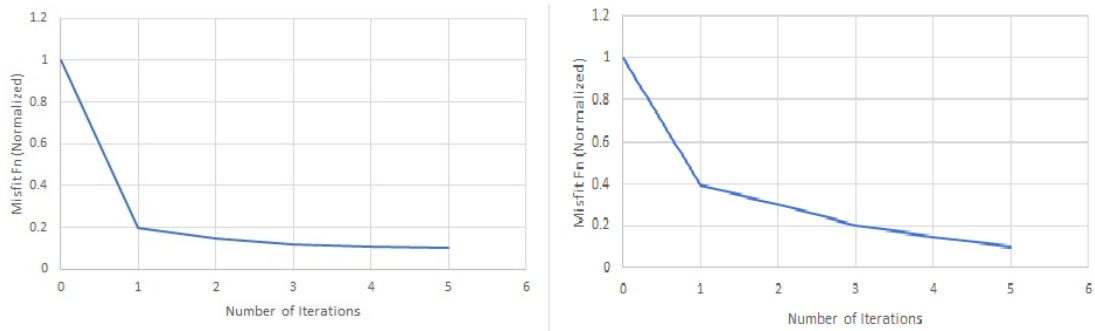

Figure 12 Misfit function vs number of iterations for the checkerboard test (left) and the field data (right).

The trials with the tomography package continued with the checkerboard tests and the latitudinal and longitudinal slices through the initial velocity model. For comparison with the 1964-1967 period, we decided to display again the E-W and N-S slices that intersected closest to an approximate city center point with coordinates 42°N and 21.5^{o}E (Figure 13).

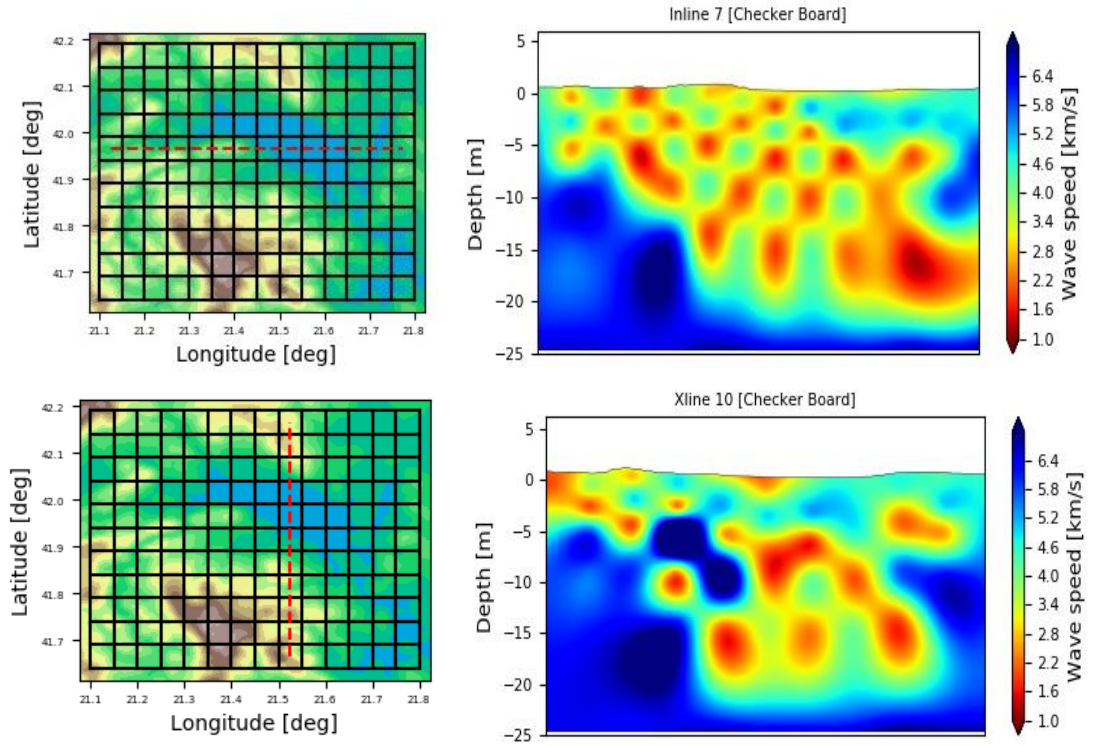

Figure 13 Recovered checkerboard images for the slices (dashed line on the left side) in respect to the initial velocity model; (Blue-fast, Red-Slow).

The most southerly and westerly slices in the cuboid had insufficient ray coverage to change the background velocity model. The images produced using the P- and S-arrivals looked very similar too, due to the fact that the number of readings used in the

inversion was very close in both cases. The results from the third to the tenth slices of the cuboid can be viewed with higher confidence because they had relatively good angular coverage. Since the deepest earthquake that occurred in the 2016-2020 period was 27km down, only the voxels in the upper layers of the volume were sufficiently covered by the seismic rays, while the deeper part may experience the artefacts of tomography. Voxels in the bottom layer which were not criss-crossed by rays were left unchanged to their initial values in the velocity model, because no extra information was added.

Lastly, we produced the tomography images with the field data for the selected longitudinal and latitudinal sections through the model. Although tomography slices can be represented in other directions, we considered the same two E-W and N-S sections that intersected closest to the point 42°N and 21.5^{o}E. Figure 14 shows the images of relative slowness perturbation in terms of a percentage change within the layers.

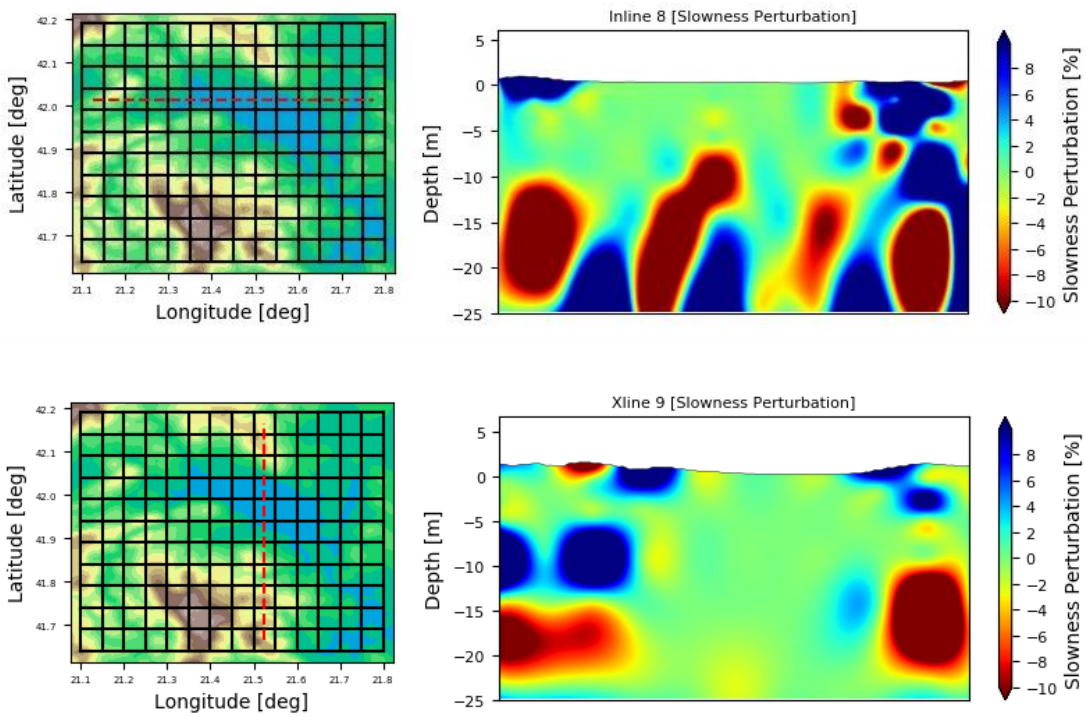

Figure 14 Slowness perturbation images of field data for the slices (dashed line on the left side) as percentage values from the initial velocity model; (Blue-High, Red-Low).

After we used tomography to image the volume in 3-D and to detect anomalies in the layers, in the last step, the output velocity model from the inversion was employed to relocate the seismic events. Multiple combinations of initial models and arrival times types were tried in the relocation process. The first series of computer runs was completed using the extended 1-D models of Table 2 into layers of constant velocity. The second series of runs was done with a computer generated 3-D model consisting of interpolated velocity values from the initial model, used at the start of iterations and called proxy model. All series were performed with the selected P- and S-arrival times. Sample distribution of the original versus relocated events for two search spacings and picking precision of $\pm$0.1s is presented on Fig. 15.

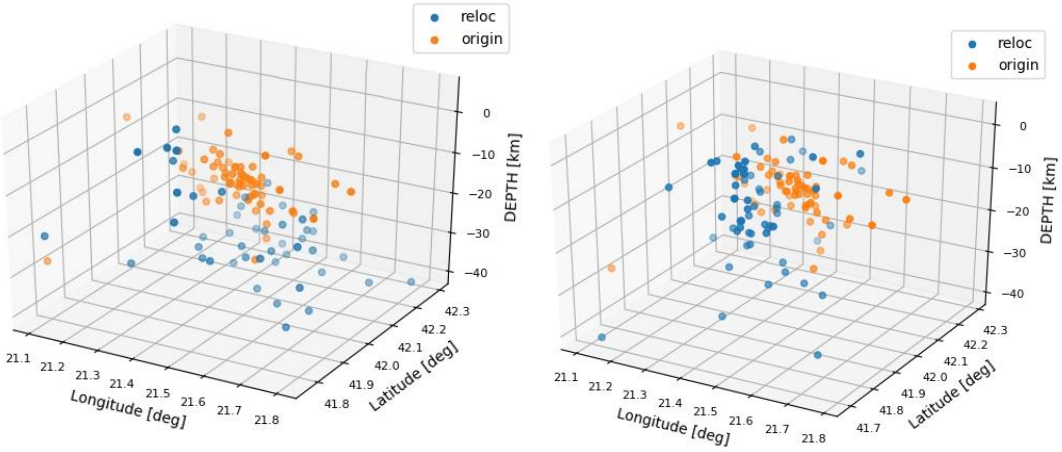

Figure 15 Distribution of the original (orange dots) versus relocated (blue dots) events for search spacing steps of 5km (left) and 1km (right) using the extended 1-D model with P-arrivals. (Mixed colour dots when original and relocated position coincided).

From these tomography images it was noticed that the third and fourth layer (10-20km) had higher values by 2-4% than the initial velocity model underneath Skopje Valley. Such anomaly causes a downwards trend of the relocated events, which confirms the previous findings that the results are strongly influenced by the geology of the top layers. Therefore, our proxy 3-D model based on the extended 1-D model is more appropriate to be used locally in the smaller scale studies.

5 DISCUSSION AND SUMMARY

This novel geotomography technique was applied to data from the epicentral area around capitol of Macedonia - Skopje, using selected earthquakes that occurred over a period of 57 years and were recorded on temporary and permanent seismograph stations. In the study we tested the tomography method to investigate the crustal shape and structures in a complex tectonic environment using specially designed datasets covering periods between 1964-1967 and 2016-2020. The two strongest earthquakes which occurred in those periods were the devastating July 1963 magnitude M_L6.1 earthquake and the September 2016 magnitude M_L5.3 event.

The present research was a continuation on the work done in the aftermath of the series of earthquakes in 2016, that dealt with the patterns of seismicity in the Skopje zone (Chernih-Anastasovska *et al.*, 2018, and Sinadinovski *et al*, 2019b). We reproduced some of the previous tomographic images and expand the analysis with the updated dataset.

The tomography and relocation results are comparatively stable and reflect the limitation of the source-receiver geometry and discretisation of the velocity model. It has to be mentioned that more interactive options are possible with the software, such as sub-zoning, which allows introduction of *a priori* assumptions from geology and helps in constraining the velocity model.

When compared, the apparent differences in seismicity pattern between the two selected periods were first in the distribution of the epicenters. In the earlier period (1964-1967), the earthquakes clustered predominantly in the NW-SE direction, along

river Vardar, on a border between two tectonic blocks. In the later period of 2016-2020, the earthquakes were more spread and moved to the north with epicenters aligning in the E-W direction. Stacked N-S tomography slices from the recent period up to 2020, showed a dipping velocity anomaly towards NNE. The hypocenter locations and the angle of dipping could be more precisely resolved if the proxy 3-D velocity model is used with a 4-5% velocity increase in the layers between 10 and 20km.

These findings are in line with the reports published by the Skopje Seismological Observatory group, who found that the seismicity in the studied area was due to the activity of approximately NW-SE and E-W oriented faults. Their analyses showed that the strongest earthquakes were caused by the seismic activity of the feature named the Skopje–Kustendil fault, which is striking roughly E-W and dipping toward NNE.

By comparison of the detailed macroseismic maps of the Skopje 1963 earthquake and the Skopje 2016 earthquake and the hypocenter depths of both, it may be also assumed that their origins were on different parts of the tectonic blocks as initially defined by Arsovski and Hadžievski (1970).

The results of the tomography inversion are reliable merely in the areas with good ray coverage. Only the parts criss-crossed by dense ray paths should be considered for interpretation, while the edges are probably influenced by artefacts. Voxels which were not covered by rays were set to keep their values as in the initial velocity model, because no additional information was available for them. In general, the tomographic images are always better resolved under the network of stations, while the uncertainty increases with the distance from the closest station.

Events outside the network area cannot be uniquely located if only the travel-time is used. An improved approach to constrain the tomography images would be consideration of the 3-component records and polarization test to narrow the azimuth of the incoming waves at the stations, which in terms of computing may speed up the search algorithm of the location objective function.

It should be emphasised that besides the velocity model, the focal depth is an important parameter for seismic hazard assessment and consequently can influence the recommended design spectra for the regions. Focal depth is the parameter with the highest uncertainty in locations using whole Earth models used by international seismological centres. In exploration geophysics, the positions of the sources and the receivers are known with certainty, accordingly the validation of the inversion results from controlled experiments would be much easier task.

A full set of trials with the tomography program has been run over a few months' time. Given the size of the output results and the limitation for publication, the authors plan to upload and link them to separate projects.

More certain interpretations can be achieved with longer term deployment of seismic instruments and increased number of recorded earthquakes. With this new tomography suite, we are now able to run the software for various tasks and display the resulting images in formats suitable for further research such as the regional earthquake hazard and risk assessment studies.

6 REFERENCES

Arsovski, M., and Hadžievski, D. (1970). Correlation between Neotectonics and Seismicity of Macedonia. Tectonophysics, 9, Amsterdam, Holland.

Chernih-Anastasovska D., Pekevski L., Drogreshka K., and Najdovska J., (2018). Seismic activity in Skopje epicentral area: past, present and future, European Seismological Commission, September 2-7, Valetta, Malta.

Kennett, B.L.N., and Abdullah, A. (2011). Seismic wave attenuation beneath the Australasian region, Australian Journal of Earth Sciences, 58, pp. 285-295.

Pekevski, L., Dojcinovski, D., Panza, G.F., Vacari, F., and Romaneli, F. (2009). Neodeterministic Seismic Hazard Analysis of the Territory of Republic of Macedonia. International Centre for Theoretical Physics November Seminar, Trieste, Italy.

Rawlinson, N., (2008). Seismology Lecture Notes: Earthquake relocation. Research School of Earth Sciences, Australian National University, Canberra, ACT.

Sinadinovski C., McCue K.F., Abdullah A. and Pekevski L., (2019a). Geotomography Trials on the Edge of the Australian and European Plates. AEES Conference, Newcastle, NSW, paper 12.

Sinadinovski C., Pekevski L., Cernih D., Drogreska K., Cejkovska V., Dojcinovski D. and Najdovska J., (2019b). Analysis of Records from the Magnitude 5.2 September 2016 Skopje Earthquake, European Geosciences Union EGU, April 7-12, Vienna, Austria.

Sinadinovski C., Pekevski L., Abdullah A. and McCue K.F., (2020). Seismic Tomography of Macedonia, European Geosciences Union EGU virtual, May 4-8, Vienna, Austria.

UNDP/UNESCO: (1974). UNDP/UNESCO Survey Seismicity of the Balkan Region: Map of Earthquake Origin Zones. UNESCO, Skopje, Macedonia.